Nano-indentation Testing for Al-Cu Bulks

Fabio Maugeri*, Giuseppe D' Arrigo†, and Michele Calabretta‡
*Department of Electrical, Electronics, and Informatics Engineering, University of Catania, Catania Italy
†CNR-IMETEM, Italy, Str. Primosole, Catania Italy
‡STMicroelectronics, Str. Primosole, Catania Italy

***Abstract*—The present paper provides a practical method for rapid evaluation of the mechanical properties of a copper specimen, avoiding long and onerous fatigue analysis. Instrumented indentation (also known as relative penetration depth) is used to calibrate and validate a finite element (FE) analysis simulation model using COMSOL Multiphysics. The selected tool (CSM Nano Scratch Tester) allows for the validation of the FE model, providing for the individual characteristics of the contact point and penetration depth with remarkable accuracy (in the order of $10^{-11}m$). The validated FE model enables to determine the stress state originating from the indentation test and the pile up on the specimen for loads in the range 0 to 300 mN.**

***Keywords*-Nanoplasmonics, FEM, Surface Plasmon Polariton**

I. Introduction

Recently nanofabrication is gaining a great interest and several methods have been recently developed for studying phenomena and developing tools at nanoscale [1].

Indentation is a non-destructive method which is widely used to estimate mechanical properties of small volumes of material. It requires high forces, thus such diamond penetrators as Vickers or Berkovich tip are applied. However, precise results can be obtained only if the penetrators geometry is well defined, as well as the exact position of the contact point is established. A penetrator can present certain roundness due to the use and the presence of dust, which can significantly influence the indentation curve.

Often, due to minor geometrical irregularities, the four facets of a Vickers tip form a line rather than meet at a single point. For this reason, the present study describes the nano-indentation hardness test of a copper specimen using a Berkovich indenter tip. A high resolution instrument (CSM Nano Scratch Tester) has been employed to continuously register the loads and displacement of the penetrator during the loading-holding-unloading cycle with a remarkable accuracy of one hundredth of a nanometer ($10^{-11}m$).

The resulting indentation curve has been analysed using Oliver and Pharr method, whereas the FE model offers a load curve with great precision. From the obtained indentation curves (elastic and plastic field) one can yield different mechanical characteristics (e.g. hardness, Youngs modulus, etc.).

II. Indentation using a Berkovich tip

The geometrical characteristics of the diamond penetrator Berkovich are shown in Fig. 1.

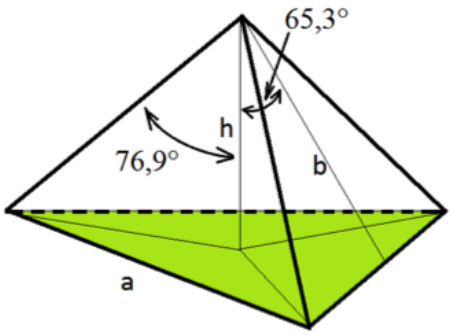

Fig. 1. Berkovich tip geometrical characteristics.

- Angle at the vertex between the probe axis and each edge 76.9^o.
- Angle at the vertex between the probe axis and the opposing face 65.3^o.
- Triangle at the base is equilateral

The dimension of the impression surface once the load is removed is calculated as follows:

$$H = \frac{P_{Max}}{A} \tag{1}$$

where P is the test force in mN and A is the surface area in μm^2. The latter is calculated via optical microscope available in the CSM Nano Scratch Tester. The change in loads and displacement allows us to obtain the indentation curve. In particular, displacement depends on the parameters which can be obtained by using Oliver and Pharr method. Specifically, in case Berkovich indenter tip is employed, the projection of the contact surface is related to the penetration depth via the following formula:

$$A = \pi \cdot tan^2(70.3) \cdot h_C^2 = 24.5 \cdot h_C^2 \tag{2}$$

Penetration depth results from:

$$h_C = h_m - h_s \tag{3}$$

where h_m is the maximum penetration and h_s is the vertical displacement of the surface at the perimeter of the contact and thus can be obtained from the general Sneddon equations for indenters of any shape, always expressed as:

$$h_s = \epsilon \frac{F_m}{S} \tag{4}$$

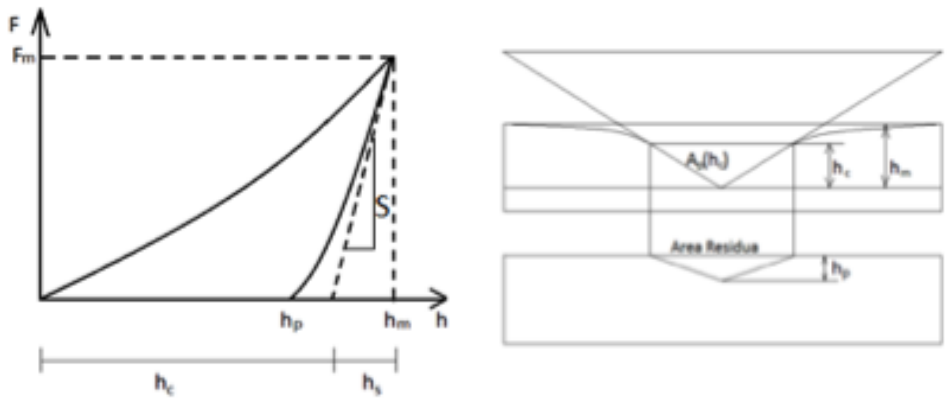

Fig. 2. Lateral view of the Indentation curve and Penetration.

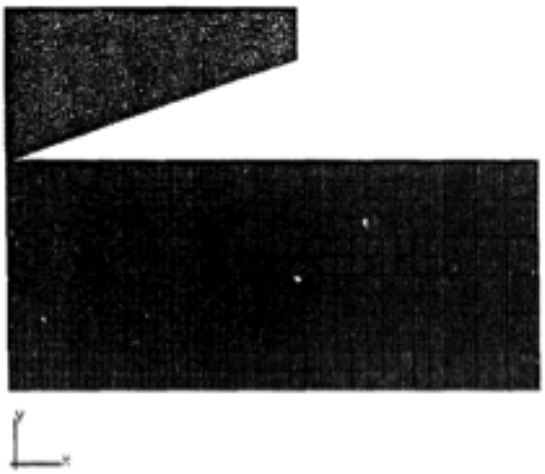

Fig. 3. Mesh of the whole sample with the indenter modeled as a movable rigid surface.

where ϵ is a factor dependent only on the indenter's geometry.

III. Geometrical Model

The present study offers a 3D Berkovich hardness model illustrating one third of the original geometry (see Fig. 3). The base of the penetrator is modelled as an isosceles triangle with the base $129.9\mu m$ and sides $75\mu m$. The specimen is modelled as a prism with a triangular base similar to the penetrator base and height $75\mu m$. The contact point (for the sake of convenience) bears the following coordinates (x;y;z)=(0;0;0).

IV. Axisymmetric Model

In order to define an axisymmetric model, we have used an equivalent conical indenter with a semi-apical angle of $\theta = 70^o30'$. This system has geometric and loading symmetry around the axis of the indenter. The specimen is modeled with 2635 4-node axisymmetric reduced integration elements (CAX4R element type).

The indentation region is very small with respect to the size of the sample. A high mesh refinement is used for modeling the large deformation area. In the outer zones multi-point constraints (MPCs type linear) are introduced lot interfacing one element with two adjacent elements to reduce the total number of degrees of freedom.

Finally, semi-infinite elements (CINAX4 clement type) resemble the far field domain in the radial direction. The elements at the interlayer between the film and the substrate are reduced in height to be able to more accurately detect the behavior of that zone. The imposed geometrical boundary conditions are: the nodes along the axis of rotation can move only along such an axis, i.e. the y axis; and all the nodes on the bottom of the mesh are fixed, i.e. the displacements along x and y direction, are constrained [2], [3], [4], [5], [6].

An important feature of COMSOL is its capability to model the contact between two bodies as a sliding through contacting surfaces, which arc in our case the indenter surface and the specimen surface. The damping coefficient was calculated with the same procedure reported in [5], [6]. From the initial geometry the nodal gaps between the surfaces are defined.

During the analysis, the program controls the variation of the nodal gaps. In particular whenever the distance between the indenter and the specimen becomes zero gap closure the contact takes place and an external reaction force is exerted on the nodes involved in the contact. The contact constraint is enforced by tile definition of the master and the slave surfaces, only the master surface can penetrate into the slave surface and the contact direction is always taken as being normal to the master surface. We have chosen the indenter surface as the master surface due to the larger stiffness of the indenter with respect to the specimen. In Fig. 2 the indenter is represented by a rigid movable surface. Since the coating is very hard, we have also modeled the tip with axisymmetric elements to take into account the stiffness of the indenter.

This mesh is shown in Fig. 3. The friction coefficient between the tip and the specimen surface is assumed to be zero, because in the case of a hard coating on a softer substrate, like TiN/HSS system, the friction has a negligible effect on

the nanoindentation process.

Coating and substrate are assumed to be initially stress free and in perfect contact during the indentation process. Both the TiN coating and the HSS substrate are assumed to be homogeneous and isotropic and having a perfect elastic-plastic behavior [7], [8], [9], [10], [11], [12].

The indentation procedure is simulated by two subsequent steps: loading and unloading. During loading, the rigid surface or the modeled tip moves along the y direction (see Fig. 2 and 3) and penetrates the specimen up to the maximum depth; during unloading, the tip returns to the initial position. At each depth increment, the program makes many iterations according to a specified convergence rate to reach an equilibrate and congruent configuration [13], [14], [15], [16], [17].

Purely elastic deformation takes place only during the beginning of the indentation process. The Mises yield criterion is applied for determining the occurrence of the plastic deformation. The equivalent Mises stress is given by the expression:

$$\sigma_{Mises} = \sqrt{\frac{(\sigma_1 - \sigma_2)^2 + (\sigma_2 - \sigma_3)^2 + (\sigma_3 - \sigma_1)^2}{2}} \quad (5)$$

where $\sigma_1,\ \sigma_1,\ \sigma_1$ are the three principal stresses. Whenever σ_{Mises} reaches the yield strength σ_0, the material begins to deform plastically.

V. Elastoplastic model of Copper Specimen

The specimen to be indented is copper, while the Berkovich indenter tip is diamond (extremely hard material) so as not to suffer significant deformation during indentation process. Diamond indenter operates only in elastic field and is characterised by Young's modulus, density and Poisson's ratio: Diamond E =1141 GPa; $\rho = 3530 kg/m^3$; $\nu = 0.07$.

The copper specimen will be subjected to stresses leading to permanent deformation, thus, elements characterizing elastoplastic behaviour of materials must be added to the three previously mentioned characteristic dimensions. Copper E =125 GPa; $\rho = 8920 kg/m^3$; $\nu = 0.34$. In order to do that, Ramberg-Osgood law must be applied:

$$\sigma = K\epsilon_p^n,\ for\ \sigma \geq \sigma_{sn} \quad (6)$$

- σ_p plastic strain.
- σ stress in the corresponding direction.
- K material constant which corresponds to the value of σ at $\sigma_p = 1$.
- n hardening behaviour of the material.
- σ_{sn}yield strength.

For copper, such values have been obtained in literature: $K = 530$, $n = 0.44$, $\sigma_{sn} = 70 MPa$.

VI. Boundary Condition

The following boundary conditions have been introduced:

1) Symmetry in compliance with the symmetrical plane of the model;
2) Fixed constraint τ at the base of the model;

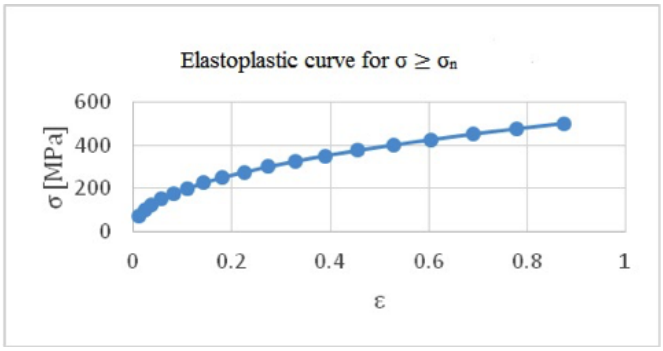

Fig. 4. Elastoplastic curve for $\sigma \geq \sigma_{sn}$.

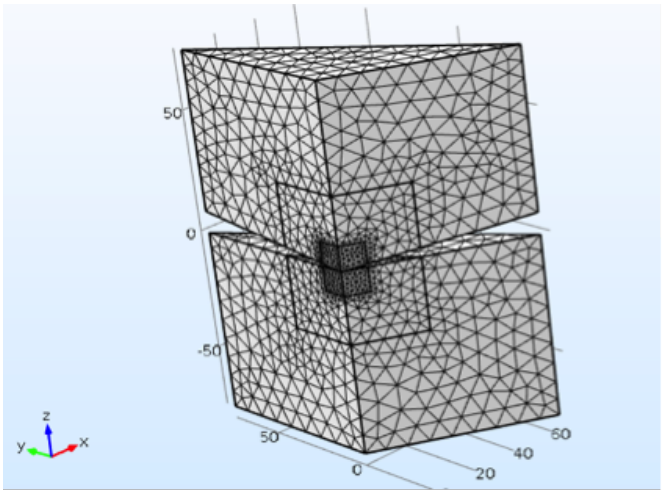

Fig. 5. Differential mesching in Berkovich.

3) Kinematical constraint in z direction of the indenter tip (null displacement in x and y directions);
4) Kinematical constraint in z direction of the axis intersecting the contact point, belonging to both the indenter and the specimen;
5) All other boundaries are considered to be unconstrained.

A. Mesh Generation

Being exclusively composed of tetrahedrons, mesh is defined with greater attention in the area surrounding the contact point. The three dimensional domains are organized in pairs [18], [19] in the following way:

- every pair includes equally dimensioned domains in x and y direction (except for the pair of domains located furthest from the contact point);
- the pairs are numbered from 1 to 3 (ranging from smallest to largest dimensions);
- Maximum dimension of the elements $2\mu m$;
- Maximum dimension of the elements $6\mu m$;
- Maximum dimension of the elements $9\mu m$;

VII. Solution Strategy

The geometrical model is based on the load that acts vertically on the base of the Berkovich tip using stationary

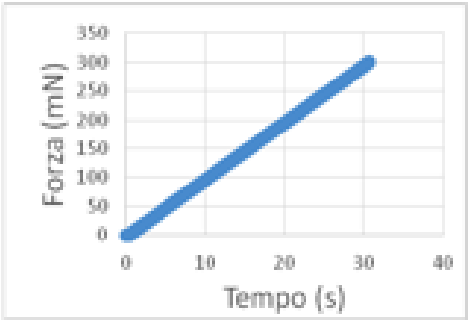

Fig. 6. Load versus Time.

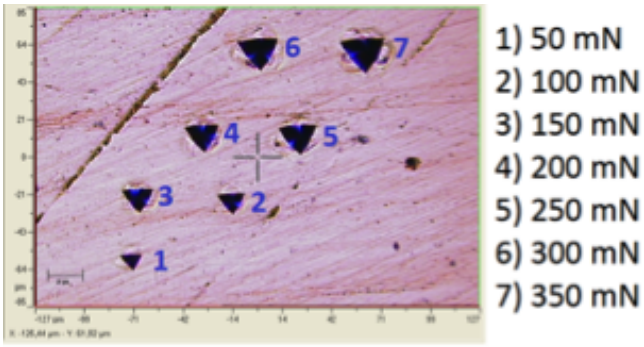

Fig. 7. Indentation test on copper specimen.

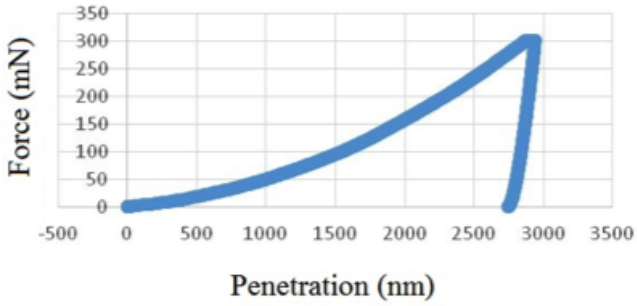

Fig. 8. Load versus penetration.

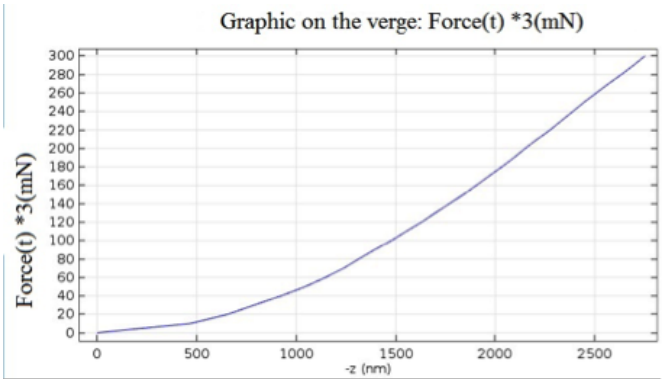

Fig. 9. Graphic on the verge.

analysis and parametric solver from the Structural Mechanics module in Comsol Multiphysics 5.1. This option is set up to facilitate dynamic analysis that depends on the variation of load in time. The final solution is sought interactively from a series of multistage elastoplastic static solutions generated under the control of variable displacement parameter. In every phase, the geometrical configuration is calculated using the previous one. The load is measured within the range of 30 seconds (during which the maximum load of 300 mN is achieved) with a step being 1s.

VIII. Contact between Parts

In COMSOL Multiphysics the problem of contact between parts is solved by determining the initial contact pair, i.e. source and destination. In this case, penetrator is considered to be the source, whereas the specimen is the destination. The problem of contact between parts is thus solved by using Penalty method with the offset null penalty function. Examining the case of maximum load being 300 mN, the following curve is obtained (see Fig. 8 and 9).

IX. Copper Specimen

Prior to carrying out the test, it is necessary to choose the solid specimen surface (by using electronic microscope) that does not have visible depressed areas or ridges which could influence the test result. Several indentation tests are then carried out on a copper specimen in seven different points with the maximum load ranging from 50 mN to 350 mN (i.e. a step being 50 mN) and dwell time 10 seconds.

Examining the case of maximum load being 300 mN, the following curve is obtained (see Fig. 10 and 11).

X. Results

The numerical analysis on the model at 51330 degrees of freedom (plus 436590 internal DOF) provides the following curves. Estimated indentation curves indicate a mutual agreement if compared to their experimental counterparts. A prior validation test versus the experimental values is assessed by juxtaposition of the load curves.

Fig. 10 (left) shows Von Mises stress state originating from the point of maximum contact from a lateral perspective, while Fig. 10 (right) indicates the stress state on a copper specimen (maximum value being the contact point between the edge of the tip and the specimen).

Moreover, the shape of the impression (Fig. 11 (right)) can be evaluated from a lateral perspective (in a section along the contact point) in the direction perpendicular to the direction of the applied load, passing by the vertex of the triangular base of the pyramid as shown in Fig. 11 (left), with the maximum pile up value being 35 mN and load 150 mN.

Moreover, the shape of the impression (Fig. 12 (right)) can be evaluated from a lateral perspective (in a section along the contact point) in the direction perpendicular to the direction of the applied load, passing by the midpoint of the triangular base of the pyramid as shown in Fig. 12 (left), with the maximum pile up value being 64 mN and load 120 mN.

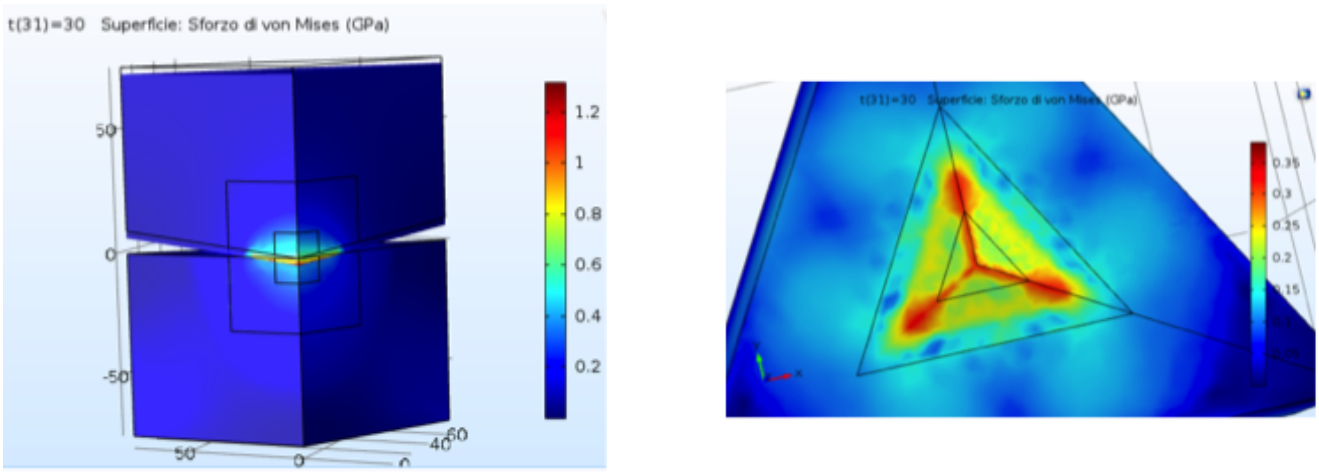

Fig. 10. Simulations of Von Mises stress.

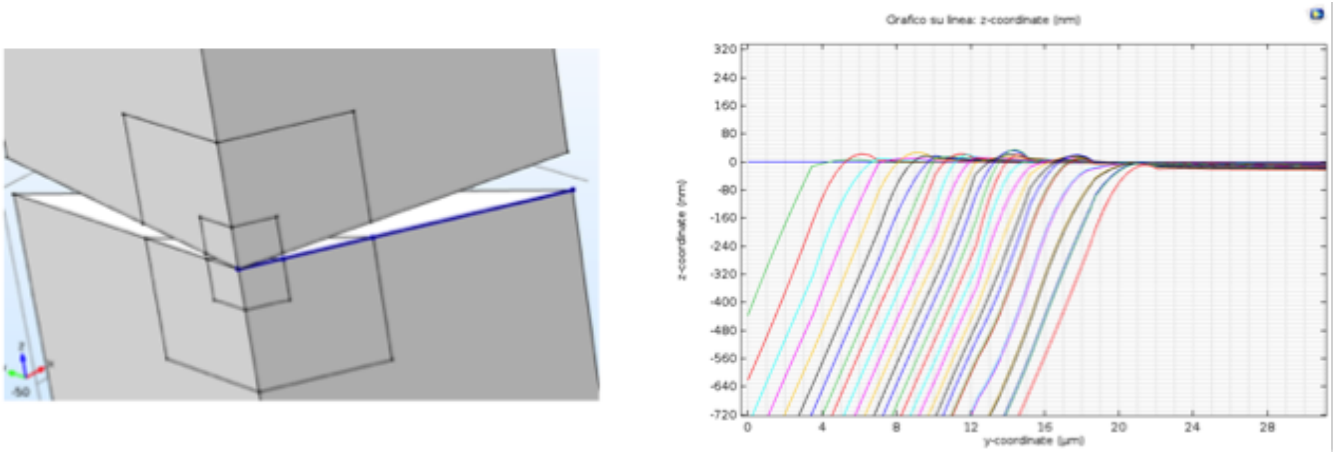

Fig. 11. Shape of the impression from a lateral perspective (passing by the vertex).

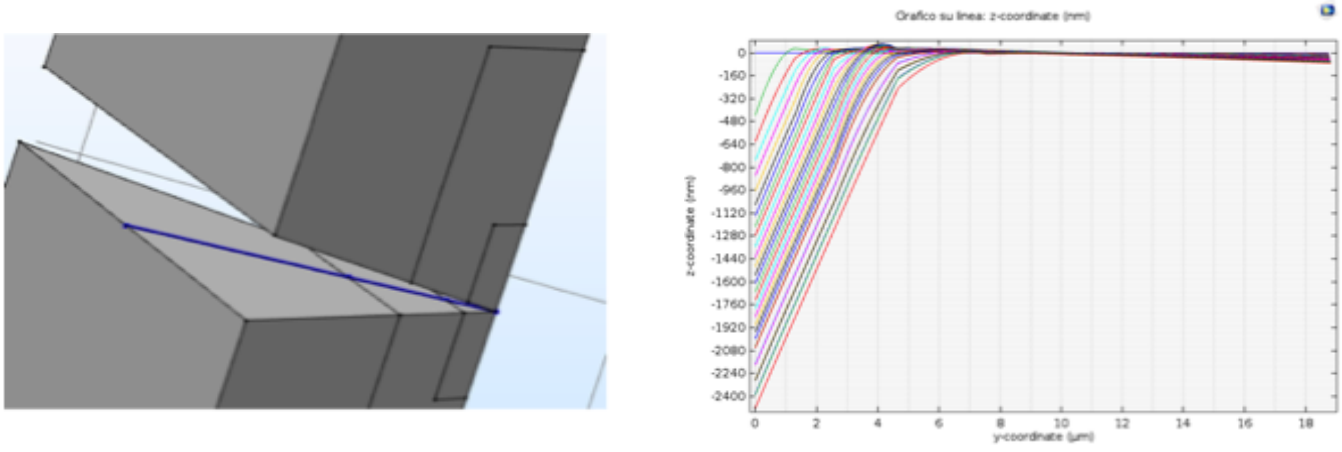

Fig. 12. Shape of the impression from a lateral perspective (passing by the the midpoint).

XI. Conclusion

The present study offers a numerical model able to manage and predict strong singularities on the contact point between the indenter tip and the specimen in a nano-indentation test. By means of suitable parameters and modelling strategies, the developed model allows a more accurate representation of the indenter tip geometry and materials in contact with it [20], [21], [22], [23], [24].

The model allows evaluating the relation between the load-penetration curve parameters and the stress state inside the specimen using the Oliver-Pharr method. The present paper is a preliminary study of a precise evaluation of the pile-up phenomenon which occurs in the microelectronic circuits. Further studies might introduce advanced neural network based models, as e.g. in [25], [26], [27], [28].

REFERENCES

[1] G. Capizzi, G. Lo Sciuto, C. Napoli, and E. Tramontana, "A multithread nested neural network architecture to model surface plasmon polaritons propagation," *Micromachines*, vol. 7, no. 7, p. 110, 2016.

[2] X. Li and B. Bhushan, "A review of nanoindentation continuous stiffness measurement technique and its applications," *Materials characterization*, vol. 48, no. 1, pp. 11–36, 2002.

[3] F. L. Savio, E. Pedullà, E. Rapisarda, and G. La Rosa, "Influence of heat-treatment on torsional resistance to fracture of nickel-titanium endodontic instruments," *Procedia Structural Integrity*, vol. 2, pp. 1311–1318, 2016.

[4] M. Calì, G. Sequenzia, S. Oliveri, and G. Fatuzzo, "Meshing angles evaluation of silent chain drive by numerical analysis and experimental test," *Meccanica*, vol. 51, no. 3, pp. 475–489, 2016.

[5] G. Sequenzia, S. Oliveri, and M. Calì, "Experimental methodology for the tappet characterization of timing system in ice," *Meccanica*, vol. 48, no. 3, pp. 753–764, 2013.

[6] M. Calì, D. Speranza, and M. Martorelli, "Dynamic spinnaker performance through digital photogrammetry, numerical analysis and experimental tests," in *Advances on Mechanics, Design Engineering and Manufacturing*. Springer, 2017, pp. 585–595.

[7] E. Pedullà, F. Lo Savio, S. Boninelli, G. Plotino, N. Grande, E. Rapisarda, and G. La Rosa, "Influence of cyclic torsional preloading on cyclic fatigue resistance of nickel–titanium instruments," *International endodontic journal*, vol. 48, no. 11, pp. 1043–1050, 2015.

[8] W. C. Oliver and G. M. Pharr, "An improved technique for determining hardness and elastic modulus using load and displacement sensing indentation experiments," *Journal of materials research*, vol. 7, no. 06, pp. 1564–1583, 1992.

[9] G. Pharr, W. Oliver, and F. Brotzen, "On the generality of the relationship among contact stiffness, contact area, and elastic modulus during indentation," *Journal of materials research*, vol. 7, no. 03, pp. 613–617, 1992.

[10] G. Sequenzia, S. Oliveri, M. Calabretta, G. Fatuzzo, and M. Cali, "A new methodology for calculating and modelling non-linear springs in the valve train of internal combustion engines," SAE Technical Paper, Tech. Rep., 2011.

[11] E. Pedulla, F. L. Savio, G. Plotino, N. M. Grande, S. Rapisarda, G. Gambarini, and G. La Rosa, "Effect of cyclic torsional preloading on cyclic fatigue resistance of protaper next and mtwo nickel–titanium instruments," *Giornale Italiano di Endodonzia*, vol. 29, no. 1, pp. 3–8, 2015.

[12] M. Calì and F. Lo Savio, "Accurate 3d reconstruction of a rubber membrane inflated during a bulge test to evaluate anisotropy," in *Advances on Mechanics, Design Engineering and Manufacturing*. Springer International Publishing, 2017, pp. 1221–1231.

[13] S. Oliveri, G. Sequenzia, and M. Calì, "Flexible multibody model of desmodromic timing system#," *Mechanics based design of structures and machines*, vol. 37, no. 1, pp. 15–30, 2009.

[14] W. C. Oliver and G. M. Pharr, "Measurement of hardness and elastic modulus by instrumented indentation: Advances in understanding and refinements to methodology," *Journal of materials research*, vol. 19, no. 01, pp. 3–20, 2004.

[15] M. A. Meyers, A. Mishra, and D. J. Benson, "Mechanical properties of nanocrystalline materials," *Progress in materials science*, vol. 51, no. 4, pp. 427–556, 2006.

[16] E. Pedullà, F. L. Savio, S. Boninelli, G. Plotino, N. M. Grande, G. La Rosa, and E. Rapisarda, "Torsional and cyclic fatigue resistance of a new nickel-titanium instrument manufactured by electrical discharge machining," *Journal of endodontics*, vol. 42, no. 1, pp. 156–159, 2016.

[17] R. Cagliero and G. Maizza, "Influence of vickers indenter tip geometry on the macro-indentation properties of γ-tial alloys."

[18] F. Bonanno, G. Capizzi, S. Coco, A. Laudani, and G. Lo Sciuto, "A coupled design optimization methodology for li-ion batteries in electric vehicle applications based on fem and neural networks," in *Power Electronics, Electrical Drives, Automation and Motion (SPEEDAM), 2014 International Symposium on*. IEEE, 2014, pp. 146–153.

[19] F. Bonanno, G. Capizzi, and G. Lo Sciuto, "A neuro wavelet-based approach for short-term load forecasting in integrated generation systems," in *Clean Electrical Power (ICCEP), 2013 International Conference on*. IEEE, 2013, pp. 772–776.

[20] J.-C. Kuo and I.-H. Huang, "Extraction of plastic properties of aluminum single crystal using berkovich indentation," *Materials transactions*, vol. 51, no. 11, pp. 2104–2108, 2010.

[21] G. La Rosa, F. L. Savio, E. Pedullà, and E. Rapisarda, "Developing of a new device for static and dynamic tests of ni-ti instruments for root canal treatment," *Procedia Structural Integrity*, vol. 2, pp. 1303–1310, 2016.

[22] B.-M. Kim, C.-J. Lee, and J.-M. Lee, "Estimations of work hardening exponents of engineering metals using residual indentation profiles of nano-indentation," *Journal of mechanical science and technology*, vol. 24, no. 1, pp. 73–76, 2010.

[23] T. Venkatesh, K. Van Vliet, A. Giannakopoulos, and S. Suresh, "Determination of elasto-plastic properties by instrumented sharp indentation: guidelines for property extraction," *Scripta materialia*, vol. 42, no. 9, pp. 833–839, 2000.

[24] Y. Liu, S. Irving, and T. Luk, "Thermosonic wire bonding process simulation and bond pad over active stress analysis," *IEEE Transactions on Electronics Packaging Manufacturing*, vol. 31, no. 1, pp. 61–71, 2008.

[25] M. Wozniak, C. Napoli, E. Tramontana, and G. Capizzi, "A multiscale image compressor with rbfnn and discrete wavelet decomposition," in *International Joint Conference on Neural Networks (IJCNN)*. IEEE, 2015, pp. 1219–1225.

[26] C. Napoli, G. Pappalardo, and E. Tramontana, "A mathematical model for file fragment diffusion and a neural predictor to manage priority queues over bittorrent," *International Journal of Applied Mathematics and Computer Science*, vol. 26, no. 1, pp. 147–160, 2016.

[27] C. Napoli, G. Pappalardo, M. Tina, and E. Tramontana, "Cooperative strategy for optimal management of smart grids by wavelet rnns and cloud computing," *IEEE Transactions on Neural Networks and Learning Systems*, vol. 27, no. 8, pp. 1672–1685, 2016.

[28] C. Napoli and E. Tramontana, "Massively parallel wrnn reconstructors for spectrum recovery in astronomical photometrical surveys," *Neural Networks*, vol. 83, pp. 42–50.